Energy 103 (2016) 807–823

Contents lists available at ScienceDirect

Energy

journal homepage: www.elsevier.com/locate/energy

A discrete and continuous mathematical model for the optimal synthesis and design of dual pressure heat recovery steam generators coupled to two steam turbines

Juan I. Manassaldi [a], Ana M. Arias [a], Nicolás J. Scenna [a], Miguel C. Mussati [a, b], Sergio F. Mussati [a, b, *]

[a] CAIMI Centro de Aplicaciones Informáticas y Modelado en Ingeniería (Universidad Tecnológica Nacional, Facultad Regional Rosario), Zeballos 1346, S2000BQA Rosario, Argentina
[b] INGAR Instituto de Desarrollo y Diseño (CONICET-UTN), Avellaneda 3657, S3002GJC Santa Fe, Argentina

ARTICLE INFO

Article history:
Received 18 July 2015
Received in revised form
20 February 2016
Accepted 22 February 2016
Available online 7 April 2016

Keywords:
HRSGs (Heat recovery steam generators)
Combined cycle power plants
Mathematical programming approaches
MINLP models
GAMS (General Algebraic Modeling System)
Optimal synthesis and design

ABSTRACT

This paper addresses the optimal arrangement and design of a dual pressure heat recovery steam generator coupled to two steam turbines. A superstructure that embeds various alternative configurations is optimized considering the following two single objective functions: (a) the maximization of the total net power generation for a given total heat transfer area and (b) the minimization of the total heat transfer area for a given total net power. The optimal number of heat exchangers and pumps and how they should be connected are the discrete decisions. The dimensions and operating conditions are the continuous decisions. A discrete and continuous mathematical model is developed and logical propositions are used for discrete decisions. The results are compared with a reference case reported by other authors. The results indicated that the optimization of the proposed superstructure allowed to find a more efficient HRSG configuration. The obtained configurations differ from the configuration of the reference case in how the heat exchangers and pumps are connected. A considerable increase in about 8% of the total net power generation in (a) and a significant reduction in about 24% of the total heat transfer area in (b) are achieved when compared to the reference case.

1. Introduction

Compared to the conventional steam and/or gas turbine power plants, the CCPPs (combined cycle power plants) offer higher thermal efficiency and are less environmental impact. In a typical combined cycle the HRSG (heat recovery steam generator) is considered to be the most important process-unit because is the link between the gas turbine-based topping cycle and steam turbine-based bottoming cycle. In the HRSG, the heat of the hot exhaust gas produced by the gas turbine is recovered and is used to convert water into steam which is then used by the steam turbines to produce power. The overall performance of the CCPPs depends strongly on how efficient the HRSG design is. The main goal and contribution of this paper is focused on the development of a mathematical model which allows the simultaneous optimization of the arrangement, size and operating conditions of the HRSG in order to optimize a given objective function. Precisely, two single objective functions are considered in order to show the applicability of the proposed model: a) the minimization of the THTA (total heat transfer area) for a fixed TNP (total net power) and b) the maximization of the TNP for a fixed THTA.

In the literature, there are many papers published addressing the mathematical modeling and optimization of heat and power plants including combined cycles. This is because of the different levels of complexity and assumptions used to derive mathematical models as design specifications are assumed, several analysis methodologies and/or optimization approaches are employed.

During the last time, several techniques based on the second law of thermodynamics, such as exergy analysis and exergoeconomic analyses have been applied in energy conversion systems.

* Corresponding author. INGAR Instituto de Desarrollo y Diseño (CONICET-UTN), Avellaneda 3657, S3002GJC Santa Fe, Argentina. Tel.: +54 342 4534451; fax: +54 342 4553439.
E-mail address: mussati@santafe-conicet.gov.ar (S.F. Mussati).

http://dx.doi.org/10.1016/j.energy.2016.02.129
0360-5442/

Exergy analysis is usually applied in a systematic way and it allows the localization and account of the inefficiency degree indicating the most inefficient components in a system. These values can be then used in the decision-making process, for instance in the retrofit of processes in order to improve the already existing process by switching out or by introducing components that involve low irreversibility. This can contribute to improvements of the thermal system as a whole or at a component level. In some cases, the exergy analysis can accurately assess the locations of inefficiencies than energy analysis. Mansouri et al. [1] investigated the effect of HRSG (heat recovery steam generator) pressure levels on exergy efficiency of combined cycle power plants and show that increases in the number of pressure levels of the HRSG affect the exergy losses due to heat transfer in the HRSG and the exhaust of flue gas to the stack. By applying the exergy analysis, Sanjay [2] investigated the effect of operating parameters on the rational efficiency and exergy destruction of combined cycle and showed that higher turbine inlet temperature and higher compressor pressure ratio is favorable on the performance of combined cycle. Regulagadda et al. [3] conducted a parametric study of a thermal power plant under various operating conditions, including different operating pressures, temperatures and flow rates, in order to determine the parameters that maximize plant performance. The exergy loss distribution indicates that boiler and turbine irreversibility yield the highest exergy losses in the power plant. Tsatsaronis et al. [4] proposed to split the exergy destruction into avoidable and unavoidable parts and demonstrate the advantages of dividing exergy destruction and economic costs into avoidable and unavoidable parts on the example of co-generative plants. Morosuk et al. [5] introduced how to calculate the parts of exergy destruction in an advanced exergy analysis which was applied to a simple gas-turbine system and they showed the potential for improvement and the interactions among the system components. Also, Tsatsatorins et al. [6] applied the advanced exergetic analysis of a novel system for generating electricity and vaporizing liquefied natural gas. The authors concluded that the application of the advanced analysis allows to obtain new improvement strategies. As the rate of exergy destruction in component A not only depends on its exergetic efficiency but also on the exergetic efficiency of the remaining components, structural coefficients are usually introduced in order to consider how local irreversibilities in the components affect the overall irreversibility rate of the cycle. These structural coefficients can only be evaluated once the irreversibilities of the components and the whole cycle are known (evaluated). Therefore, the calculation of these coefficients may require a high number of simulation runs resulting in time-consuming procedure ([7]). Certainly the simulation runs required when the process involves many unit-processes and, moreover, when the optimization problem to be solved is highly combinatorial (high number of discrete decisions) may increase drastically. Some of the recent applications of the exergy analysis in energy conversion systems can be found in Refs. [8–11].

On the other hand, thermoeconomics, also called exergoeconomics, is the combination of exergy and conventional economics. The thermoeconomic cost balance is formulated in the same way as the exergy balance but including the investment CAPEX (capital expenditure) and O&M (operating and maintenance) costs of the entire process. One of the purposes of this method is to be able to distinguish between production costs of different products, e.g. cogeneration of both heat and power. It is also used for the evaluation of cost streams and the cost of exergy destruction for individual components or the system as a whole. Exergoeconomic methods may be grouped in algebraic methods and calculus methods [12,13]. The algebraic methods use algebraic balance equations and it requires to propose auxiliary cost equations for each component which represent a subjective task. On the other hand, calculus methods use differential equations, where the system cost flows are obtained in conjunction with optimization procedures based on the method of Lagrange multipliers, which determines marginal cost. In this method, the mathematical description of the function of each component is also subjective. Based on the exergoeconomic principles, Bhargava et al. [14] analyzed a cogeneration system consisting of an intercooled reheat gas turbine, with and without recuperation. Their result provided useful guidelines for preliminary sizing and selection of gas turbine cycle for cogeneration applications. Recently, Bakhshmand et al. [15] performed an exergoeconomic analysis and optimization of a combined power plant with triple-pressure including one reheating stage. To do this, the authors implemented a simulation code in MATLAB employing an evolutionary algorithm. The objective function includes both product cost rate and cost rates associated with exergy destructions. The obtained results allowed to the authors to propose optimal criteria of performance for the studied process. It should be noted that such methodology is applicable to optimize steady state operation parameters of given CCPP, and it is not suitable to optimize the design of projected systems.

Most of the conventional exergy and exergo-economic optimization methods are iterative and subjective in nature because they require the interpretation of the designer at each iteration to determine the final configuration [16].

On the other hand, motivated by the maturity of the design-optimization methods and software as well as the advent of powerful modern computational platforms there is a really renewed interest in the application of mathematical programming and rigorous optimization approaches in a variety of industrial sectors, including the area of utility plants and combined heat and power systems. Thus, there is a great variety of interesting articles addressing different optimization mathematical models considering both discrete and continuous decisions for different optimization purposes and different ways to treat the uncertainties of the models. In fact, advanced optimization approaches and mathematical models with high number of non-linear constraints and variables have already been applied to numerous problems for achieving improvements in “real-world” heat and power designs.

There are a great variety of articles that have been recently published where classical non-deterministic and deterministic techniques are applied. Certainly, there is a great number of articles that focus on the application of SA (simulated annealing) and GA (genetic algorithms) and deterministic MINLP techniques energy conversion systems.

Simulated Annealing and Genetic Algorithm are two well-known metaheuristic algorithms for combinatorial optimization. Simulated annealing is based on a simple local search algorithm proceeds by choosing random initial solution and generating a neighbor from that solution. They are derivate-free and are well suited for high complexity problems with discontinues models and without any known sophisticated solution techniques like the combinatorial optimization problems. The optimal solutions obtained by the two algorithms are strongly dependent on the parameters required by the two algorithms. For instance, in GA, the number of generations, population, crossover rate, mutation rate and tournament size (number of individuals needed to fill a tournament during selection). In addition they are inherently sequential and hence very slow for problems with large search spaces. Both, algorithms have been successfully applied in power plants where the configurations of process-units are known (fixed).

On the other hand, the deterministic MINLP optimizations, which will be adopted in this paper, are well suitable for mathematically modeling many optimization problems that involve both

discrete and continuous decisions, especially for highly combinatorial problems. They have been successfully applied in many research areas allowing to find novel configurations of processes [17–26].

Specifically in electrical power generation plant, Bruno et al. [27] developed a MINLP model for performing structural and parameter optimization of utility plants that satisfy given electrical, mechanical and heating demands of industrial processes (steam at various pressure levels). All major conventional utility plant equipments were included in the superstructure for the MINLP model. The model predicts the optimal unit configuration and the optimal operating conditions, such as, flow-rates, enthalpies and steam turbine efficiencies. Simplified mathematical models were proposed to describe the process units. The proposed approach and MINLP model resulted to be robust and useful not only for synthesis, but also for analyzing different design alternatives. Tveit et al. [28] presented an efficient methodology to build a multi-period MINLP model for steam turbine network of a utility system. The methodology consists of several steps that include the building of a simulation model of the system, the development of regression model(s) of the system based on simulation and D-optimal design, and finally the development of a MINLP model. The results showed that the proposed methodology is capable of analyzing a relatively complex steam turbine network in a utility system. However, the authors highlight that the MINLP models developed using the methodology should be regarded as 'ad hoc' models, and have certain limitations as the models are not so flexible compared to models where all the units in the utility system are modelled in detail. Later, the same authors Tveit et al. [29] presented a deterministic MINLP model to analyze new investments and long-term operations of CHP (combined heat-power) plants in a district heating network with long-term thermal storage. As part of the results, the total annual profit, the optimal selection of process options, mass flow through the plant, and generated power in each plant were obtained. Martelli et al. [30] proposed a rigorous mathematical programming model, a linear approximation, and a two-stage algorithm in order to optimize not only the HRSG of simple combined cycles but also any HRSCs (heat recovery steam cycles) with external heat/steam sources/users and with multiple supplementary firing. The authors successfully applied the proposed model and methodology to highly integrated plants (biomass to Fischer–Tropsch liquids plants, IGCCs (integrated gasification combined cycles) with and without CCS, and coal to SNG (synthetic natural gas) facilities). Other articles related with the optimization of CHP plants using MINLP frameworks can be also found [31–35].

Despite the existence of many articles concerning with the study of natural gas combined cycle power plants under different assumptions and computational tools, there is limited research considering the optimization of such plants in where the heat exchangers layout in the HRSG is considered as an optimization variable. Certainly, only few publications deal with the optimization of the layout of the HRSG coupled into [36–39]. In this context, Zhang et al. [36] recently developed a mixed-integer nonlinear programming model for the design optimization of a HRSG with consideration of several alternative matches between the HRSG and external heat flows. The authors proposed a superstructure including different alternative layouts of HRSG and connections between the HRSG and other external heat exchangers. Then, a MINLP model is proposed and solved to determine the optimal arrangement for several case studies that included two and three pressure levels with and without steam re-heating.

In this paper, the optimal synthesis and design of a combined cycle power plant that includes a dual pressure heat recovery steam generator and two steam turbines is addressed. In this paper, "synthesis" will refer to the selection of the configuration of the heat exchangers, that is, which economizers and superheaters should integrate the optimal configuration and how they should be interconnected, implying discrete decisions. On the other hand, "design" will refer to determine the sizes (heat transfer areas, power required by pumps and power produced in the steam turbines) and operating conditions (flow-rates, pressures and temperatures) of the selected process-units, implying continuous decisions.

Precisely, a superstructure embedding not only the alternative layouts proposed by Zhang et al. [36] but also other competitive layouts is proposed for the HRSG and then the entire system (dual pressure heat recovery steam generators coupled to two steam turbines) is simultaneously optimized to determine the best configuration of the dual HRSG, the optimal operating conditions and size of each piece of equipment. Thus, the main contribution of this paper is to develop a discrete and continuous mathematical programming model that systematically selects the best HRSG configuration for any objective function (TNP or THTA) defined by the user. Moreover, the proposed model will be also useful to determine the optimal synthesis and design of integrated combined cycle power plants and processes with high energy consumptions, for instance, among others, dual purpose desalination plants in where thermal desalination systems (multi-effect or multi-flash evaporation systems) are coupled with power plants.

Finally, it should be mentioned that the data and results reported by Zhang et al. [36] will be selected as base configuration and reference data because of the fact that they obtained their results using a MINLP model and by optimized a superstructure including the layout of the HRSG in a similar way to that proposed in the current paper but proposing another way to model the discrete decisions. Thus, the configuration reported by Zhang et al. [36] can be assumed as a valuable and useful solution for comparison purpose.

The paper is outlined as follows. Section 2 introduces the problem formulation. Section 3 summarizes the assumptions and details of the mathematical model. Section 4 presents applications of the developed MINLP model and discussion of results. Finally, Section 5 presents the conclusions and future work.

2. Problem statement

Given the flow-rate and inlet temperature of the flue gas stream and the superstructure of alternative configurations shown in Fig. 1, the goal is to determine the best integration arrangement, optimal operating conditions and dimensions in order to optimize the proposed objective functions: a) maximization of the total power for a given total heat transfer area and b) minimization of the total heat transfer area for a given total power production. The optimal solutions obtained in a) and b) are hereafter named as OD1 and OD2, respectively. The optimal configuration obtained by the superstructure proposed by Zhang et al. [36] is used as a reference design. Hereafter it is named as RC and its performance will be compared to those obtained from the superstructure shown in Fig. 1. The comparison of the three optimal designs will be performed in terms of the HRSG configuration, heat transfer area and total power productions.

Regardless to the HRSG, the main difference between the superstructure proposed in this paper (Fig. 1) and that proposed in Zhang et al. [36] is the possibility of using the Pump #1 after the economizer (EC1) in the superstructure proposed in this paper (Fig. 1). The inclusion of the Pump #1 increases the number of degrees of freedom of the optimization problem, allowing to increase, if it is beneficial, the inlet pressure in the economizer#4

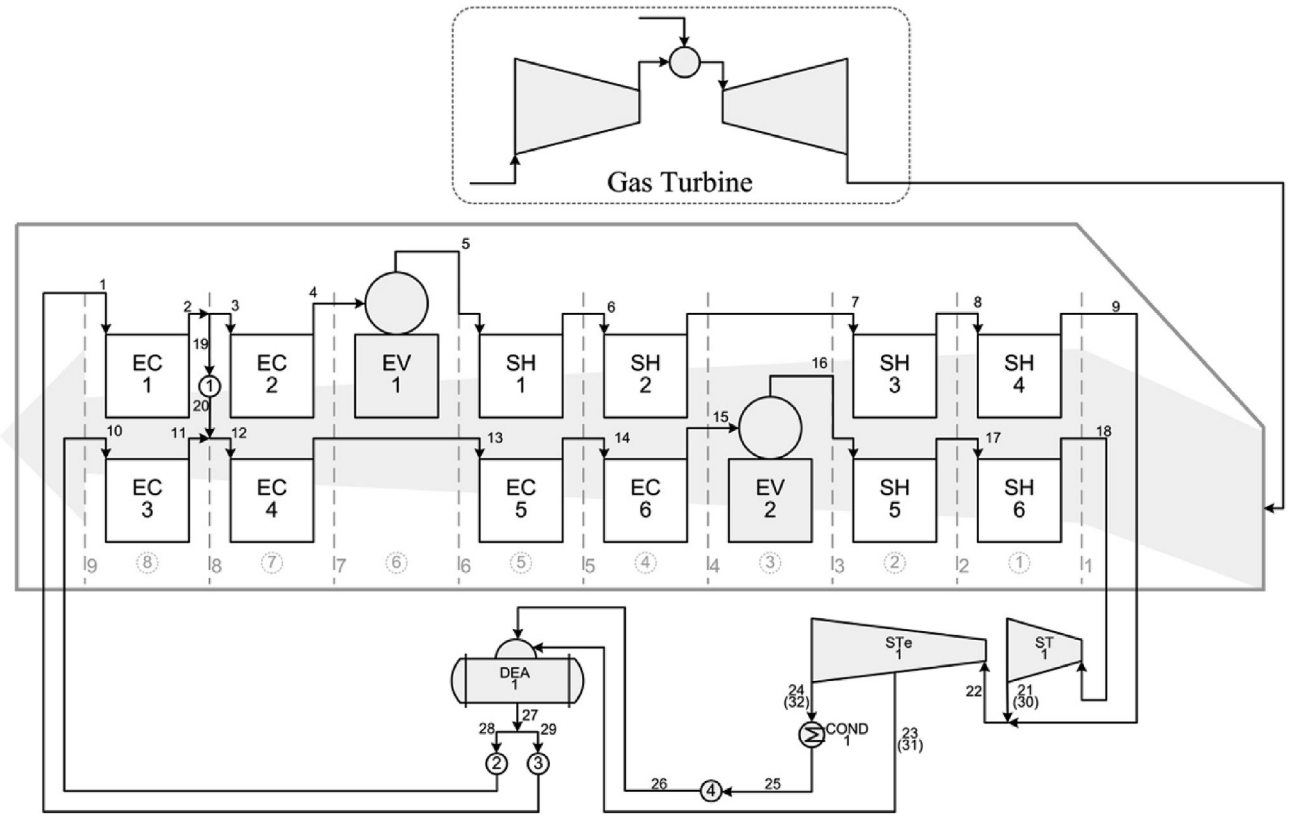

Fig. 1. Proposed superstructure embedding several alternative HRSG configurations.

(EC4), which will affect the temperatures of both the water and gas streams along of the HRSG, affecting not only the driving forces but also the heat transfer areas of the all involved heat exchangers. Another difference is that in Zhang et al. [36], the arrangement of heat exchangers for the HRSG is optimized with the aim to maximize the total power output of steam turbines which is computed in a simplified way, as a function of steam flow and steam specific enthalpy. In the current paper, the HRSG configuration obtained by Ref. [36] has been coupled to two steam turbines similarly to that shown in Fig. 1 and the total power output of steam turbines has been computed by using the same steam turbine model proposed in this paper. In addition, the deareator has been also considered in both superstructures.

As mentioned earlier, the superstructure shown in Fig. 1 embeds several alternative configurations. Fig. 2 illustrates some of the potential configurations that are embedded. For instance, in Fig. 2(a), the pump #1 is not included and the steam stream that leaves EV1 exchanges heat in the superheater#2 (SH2) with the gas stream that leaves the evaporator#2 (EV2). In contrast to Fig. 2(a), in (b) the pump #1 is included and the steam stream that leaves the evaporator#1 (EV1) exchanges heat in SH3 with the gas stream that leaves the spuerheater#6 (SH6). Another difference that can be observed between Fig. 2(a) and (b) by the inclusion of the pump #1, is that only one water stream may be fed into the HRSG in Fig 2(b). On the other hand, by comparing Fig. 2(a) and (d), it is possible to observe that the location of the SH2 is different. Certainly, in Fig. 2(a), the steam stream that leaves the EV1 exchange heat with the gas stream that leaves the EV2, but in Fig. 2(b) it exchange heat with the gas stream that leaves the EC5. Based on these comments, it is essential to determine the optimal locations of the heat exchangers taken into account the trade-offs that exist between pressures, temperatures and flow-rates which affect the requirements of pumping power and heat transfer areas as well as the power produced in each steam turbine.

3. Assumptions and mathematical model of the proposed superstructure

This section presents the key assumptions and the mathematical model developed for the superstructure of alternative shown in Fig. 1.

3.1. Assumptions

- Steady state is assumed
- The specification of the exhaust gas stream that comes from the GT (mass flow rate, temperature and composition) is known.
- Unfired and dual pressure heat recovery steam generator is considered.
- Pressure drop in the working fluid side is neglected, excluding steam turbines and pumps.
- Specific correlations taken from IPWS 97 [40] are used to compute the thermodynamic properties of water.
- Correlations taken from Ref. [41] are used to describe the dependence of the thermodynamic properties of ideal gases with temperature and pressure.
- As a first approximation, constant overall heat transfer coefficients are assumed considering different numerical values for the economizer, evaporator and superheater. The corresponding values have been taken from Casarosa et al. [42].
- Constant isentropic efficiency for the steam turbines is assumed.
- Chen's approximation instead of LMTD method is used to compute heat transfer areas for candidate heat exchangers embedded in the superstructure.

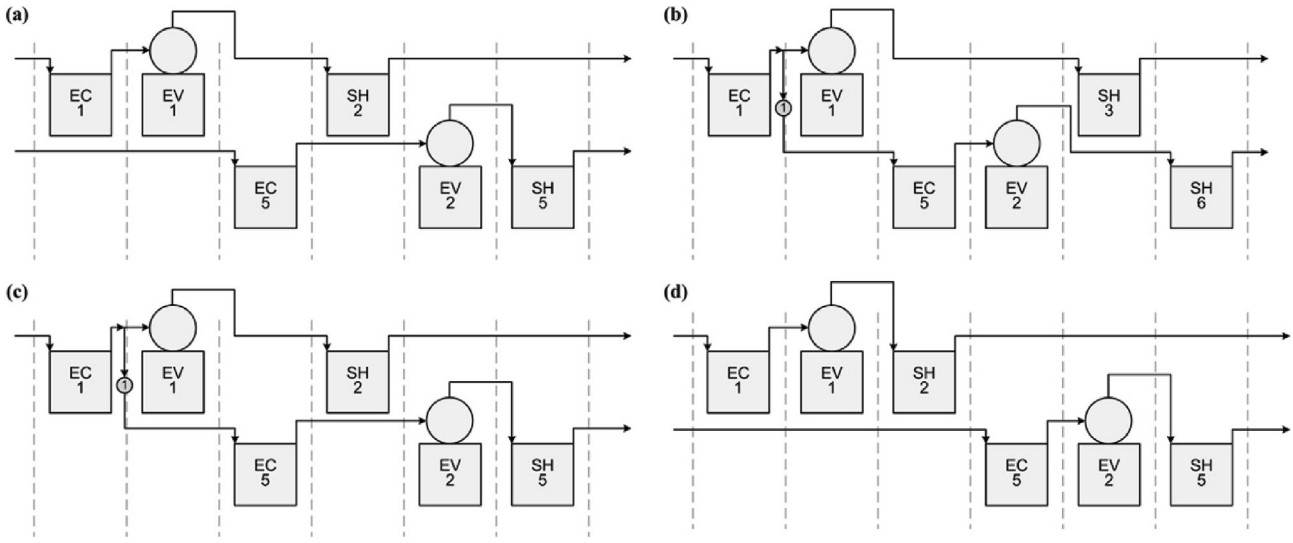

Fig. 2. Some candidate configurations embedded in Fig. 1.

- Pumping work is calculated considering water as an incompressible fluid.

3.2. Detailed mathematical model

Basically, the model includes the mass and energy balances, design equations and logical constraints related to the selection of the process units. For an easy model implementation, several sets and indexes have been defined in such a way to identify each process unit (heat exchangers, steam turbines and pumps). The notation of the mathematical programming problem follows the notation of the superstructure shown in Fig. 1. The sets EC, EV and SH refer to the economizers, evaporators and superheaters, respectively. Then, each heat exchanger in the superstructure is indexed using five indexes: n, i, j, p and q. Index "n" is used to identify the exchanger, the indexes "i" and "j" are used to denote the inlet and outlet of the working fluid stream (water) while the indexes "p" and "q" correspond to the inlet and outlet of the flue-gas stream. Based on the proposed superstructure (Fig. 1) and on the set definitions, it is easy to observe that the set EC will contain the following six economizers: EC(1,1,2,8,9), EC(2,3,4,7,8), EC(3,10,11,8,9), EC(4,12,13,7,8), EC(5,13,14,5,6) and EC(6,14,15,4,5). In a similar way, the sets EV and SH contain, respectively, two evaporators EV(1,4,5,6,7), EV(2,15,16,3,4) and six superheaters SH(1,5,6,5,6), SH(2,6,7,4,5), SH(3,7,8,2,3), SH(4,8,9,1,2), SH(5,16,17,2,3) and SH(6,17,18,1,2).

Using these basic sets, the model was implemented in an easy and compact manner as it is presented below.

3.2.1. Mass, energy and design constraints

3.2.1.1. Evaporator. According to the Fig. 3, the mass balances for the gas and working fluid streams are given by Eqs. (1) and (2).

$$m_i = m_j \quad \forall\, i,\ j \in EV(n,i,j,p,q) \tag{1}$$

$$m_p = m_q \quad \forall\, i,\ j \in EV(n,i,j,p,q) \tag{2}$$

On the other hand, the energy balance in each evaporator "n" is expressed as:

$$mH_i + Q_n^{ev} = mH_j \quad \forall n,\ i,\ j \in EV(n,i,j,p,q) \tag{3}$$

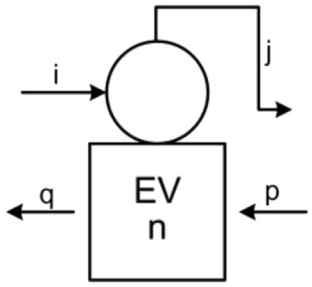

Fig. 3. Schematic representation of evaporator "n".

$$mH_p = mH_q + Q_n^{ev} \quad \forall n,\ i,\ j \in EV(n,i,j,p,q) \tag{4}$$

The heat transfer area (A_n^{ev}) is computed in terms of the heat load (Q_n^{ev}), overall heat transfer coefficient (U_n^{ev}) and driving force ($LMTD_n^{ev}$), according to the Eq. (5).

$$Q_n^{ev} = U_n^{ev} A_n^{ev} LMTD_n^{ev} \quad \forall n \in EV(n,i,j,p,q) \tag{5}$$

And the corresponding driving force ($LMTD_n^{ev}$) is calculated as follows:

$$LMTD_n^{ev} = \left((T_i^{sat} - T_q) - (T_j - T_p)\right) / \log\left((T_i^{sat} - T_q)/(T_j - T_p)\right) \quad \forall n,\ i,\ j,p,q \in EV(n,i,j,p,q) \tag{6}$$

According to the Eq. (7) the Ap (approach point) is defined as the difference between saturated steam temperature and water temperature leaving the economizer. This is one of the main model parameter and typical value widely suggested in the literature lie in the range of 8.00–16.8 K [43]. In this paper, the parameter Ap was set at 10 K, which is equal to that used in Zhang et al. [36].

$$T_i = T_i^{sat} - Ap \quad \forall\, i \in EV(n,i,j,p,q) \tag{7}$$

The working fluid (water) that leaves the evaporator is in saturated state, which is imposed as follows:

$$T_j = T_j^{sat} \quad \forall\, i \in EV(n,i,j,p,q) \tag{8}$$

3.2.1.2. Economizers. For the economizer "n" shown in Fig. 4, the mass balances are given by Eqs. (9) and (10):

$$m_i = m_j \quad \forall\, i,\ j \in EC(n,i,j,p,q) \tag{9}$$

$$m_p = m_q \quad \forall\, i,\ j \in EV(n,i,j,p,q) \tag{10}$$

The following constraint computes the heat load (Q_n^{ec}) computed from the working fluid:

$$mH_i + Q_n^{ec} = mH_j \quad \forall n,\ i,\ j \in EC(n,i,j,p,q) \tag{11}$$

The heat transfer area (A_n^{ec}) is then given by the following constraint:

$$Q_n^{ec} = U_n^{ec} A_n^{ec} \Delta T_n^{ec} \quad \forall n \in EC(n,i,j,p,q) \tag{12}$$

And the corresponding driving force (ΔT_n^{ec}) is calculated as follows:

$$\Delta T_n^{ec} = \sqrt[3]{0.5\,(T_i - T_q)\,(T_j - T_p)\,[(T_i - T_q) + (T_j - T_p)]} \quad \forall n,\ i,\ j,p,q \in EC(n,i,j,p,q) \tag{13}$$

As shown, in contrast to Eq. (6), the Chen's approximation [44] to the log-mean temperature difference is here used to avoid convergence problems especially when the optimization algorithm tries to remove some of the economizers embedded in the superstructure. In Eq. (6), the log mean temperature difference LMTD instead of the Chen's approximation has been considered because the evaporators EV1 and EV2 are assumed as fixed (EV1 in the low pressure level and EV2 in the high pressure level) and therefore they not form part of the discrete decisions.

3.2.1.3. Superheaters. In a similar way, Eqs. (14)–(18), which are expressed in terms of the set SH, refer to the mass and energy balances, heat load and heat transfer area of each superheater (Fig. 5).

$$m_i = m_j \quad \forall\, i,\ j \in SH(n,i,j,p,q) \tag{14}$$

$$m_p = m_q \quad \forall\, i,\ j \in SH(n,i,j,p,q) \tag{15}$$

$$mH_i + Q_n^{sh} = mH_j \quad \forall n,\ i,\ j \in SH(n,i,j,p,q) \tag{16}$$

$$Q_n^{sh} = U_n^{sh} A_n^{sh} \Delta T_n^{sh} \quad \forall n \in SH(n,i,j,p,q) \tag{17}$$

$$\Delta T_n^{sh} = \sqrt[3]{0.5\,(T_i - T_q)\,(T_j - T_p)\,[(T_i - T_q) + (T_j - T_p)]} \quad \forall n,\ i,\ j,p,q \in SH(n,i,j,p,q) \tag{18}$$

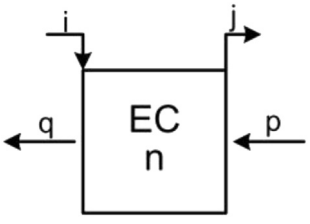

Fig. 4. Schematic representation of economizer "n".

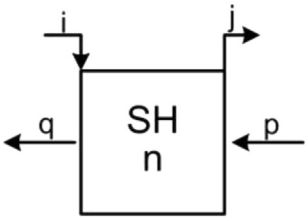

Fig. 5. Schematic representation of superheater "n".

Here, in this part of the model presentation it should be mentioned that the proposed superstructure offers interesting characteristics which have been into account in order to define three sets useful to implement and to complete the energy balances in the evaporators and superheaters in an easy and a general way. These characteristics are clearly shown in Fig. 1 and are briefly described as follows:

a) As mentioned earlier, the evaporators EV1 and EV2 are fixed in the superstructure because two pressure levels are considered.
b) At the left side of the EV1 there are two stages in where all of the heat exchangers are economizers (EC1 and EC3 in the stage 1 and EC2 and EC4 in the stage 2).
c) Between EV1 and EV2 there are also two stages. Each stage involve one superheater and one economizer (SH1 and EC5 in the stage 1 and SH2 and EC6 in the stage 2).
d) At the right side of the EV2 there are two stages in where all of the heat exchangers are superheaters (SH3 and SH5 in the stage 1 and SH4 and SH6 in the stage 2).

Then, based on these observations, the following sets have been defined *ECEC(n,n′,p,q)* (Fig. 6(a)), *SHEC(n,n′,p,q)* (Fig. 6(b)), *SHSH(n,n′,p,q)* (Fig. 6(c)) over which the energy balance required in each section of the HRSG is considered. For instance, according to Figs. 1 and 6(a), the heat transferred from the gas stream in each stage placed in the left side of EV1 is expressed as follows:

$$mH_p = mH_q + Q_n^{ec} + Q_{n'}^{ec} \quad \forall n,n',\ p,\ q \in ECEC(n,n',p,q) \tag{19}$$

Then, the energy balance that corresponds to each section of the HRSG located in the left side of the EV1 is given by the Eq. (11), which was presented earlier to compute the heat absorbed by the working fluid (water), and Eq. (19). For instance, for the stage 1, Eqs. (11) and (19) are expanded in their indexed to give the following constraints:

$$mH_1 = mH_2 + Q_1^{ec} \tag{11a}$$

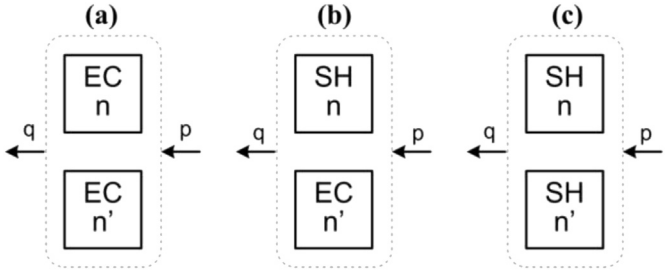

Fig. 6. Heat exchangers involved in different sections of the HRSG: (a) for sections 8 and 7, (b) for sections 5 and 4, (c) for sections 2 and 1.

$$mH_{10} = mH_{11} + Q_3^{ec} \tag{11b}$$

$$mH_8 - mH_9 = Q_1^{ec} + Q_3^{ec} \tag{19a}$$

Then, by applying a similar reasoning for the remaining stages according to their locations and defining appropriate sets (*SHEC* and *SHSH*), the next constraints can be derived for the remaining stages:

$$mH_p = mH_q + Q_n^{ec} + Q_{n'}^{sh} \quad \forall n, n', p, q \in SHEC(n, n', p, q) \tag{20}$$

$$mH_p = mH_q + Q_n^{sh} + Q_{n'}^{sh} \quad \forall n, n', p, q \in SHSH(n, n', p, q) \tag{21}$$

The Eq. (21) applies for the stages that are located between EV1 and EV2 and Eq. (22) applies for the stages located in the right side of the EV2.

3.2.1.4. Mass and energy balances in the remaining process-units. In a similar way than in the previous section, the remaining process units are also defined using sets. For example, as shown in Fig. 1 the water stream "29" enters pump "3" while the stream "1" leaves the pump. So, this equipment is defined by the sets PUMP(3,29,1). Equations for the remaining process units are listed in Table 1.

3.2.2. Logical constraints

3.2.2.1. Selection of the economizers and superheaters where the heat transfers take place. Eqs. (46) and (47) that involve binary variables are used to denote the existence of heat transfer in the economizers. If the binary variable x_n^{ec} takes a discrete value of zero then both inequality constraints become in equality constraints leading to $Q_n^{ec} = 0$. Otherwise, if the binary variable x_n^{ec} takes a discrete value of one the heat transfer is carried out and the value of Q_n^{ec} is in between the lower bound $|Q_n^{ec}|_{lo}$ and upper bound $|Q_n^{ec}|_{up}$

$$Q_n^{ec} \geq x_n^{ec} |Q_n^{ec}|_{lo} \quad \forall n \in EC(n, i, j, p, q) \tag{46}$$

$$Q_n^{ec} \leq x_n^{ec} |Q_n^{ec}|_{up} \quad \forall n \in EC(n, i, j, p, q) \tag{47}$$

Similar constraints are also proposed for the selection of the superheaters, as shown in Eqs. (48) and (49).

$$Q_n^{sh} \leq x_n^{sh} \left|Q_n^{sh}\right|_{up} \quad \forall n \in SH(n, i, j, p, q) \tag{48}$$

$$Q_n^{sh} \geq x_n^{sh} \left|Q_n^{sh}\right|_{lo} \quad \forall n \in SH(n, i, j, p, q) \tag{49}$$

3.2.2.2. Selection of the pumps. In a similar way to that proposed for the economizers and superheaters in the previous sub-section, the selection of the pumps involves binary variables y_n which are included in the following linear inequalities:

$$m_i \leq y_n |m_i|_{up} \quad \forall n, i \in PUMP(n, i, j) \tag{50}$$

$$m_i \geq y_n |m_i|_{lo} \quad \forall n, i \in PUMP(n, i, j) \tag{51}$$

Table 1
Equality constraints for the remaining process units.

$m_i = m_j$	$\forall i, j \in PUMP(n, i, j)$	(22)	
$mH_i + W_n^{pump} = mH_j$	$\forall n, i, j \in PUMP(n, i, j)$	(23)	
$W_n^{pump} = m_i v_i (P_j - P_i)$	$\forall n, i, j \in PUMP(n, i, j)$	(24)	
$m_i = m_j$	$\forall i, j \in ST(n, i, j, k)$	(25)	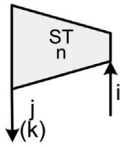
$mH_i = mH_j + W_n^{st}$	$\forall n, i, j \in ST(n, i, j, k)$	(26)	
$H_i - H_j = \eta^{st}(H_i - H_k)$	$\forall i, j, k \in ST(n, i, j, k)$	(27)	
$S_i = S_k$	$\forall i, k \in ST(n, i, j, k)$	(28)	
$m_i = m_j + m_k$	$\forall i, j \in STe(n, i, j, k, l, m)$	(29)	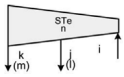
$mH_i = mH_j + mH_k + W_n^{ste}$	$\forall n, i, j, k \in STe(n, i, j, k, l, m)$	(30)	
$H_i - H_j = \eta^{ste}(H_i - H_l)$	$\forall i, j, k \in STe(n, i, j, k, l, m)$	(31)	
$H_j - H_k = \eta^{ste}(H_j - H_m)$	$\forall i, j, k \in STe(n, i, j, k, l, m)$	(32)	
$S_i = S_l$	$\forall i, k \in STe(n, i, j, k, l, m)$	(33)	
$S_j = S_m$	$\forall i, k \in STe(n, i, j, k, l, m)$	(34)	
$m_i = m_j$	$\forall i, j \in COND(n, i, j)$	(35)	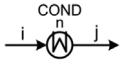
$mH_i = mH_j + Q_n^{cond}$	$\forall n, i, j \in COND(n, i, j)$	(36)	
$T_j = T_j^{sat}$	$\forall j \in COND(n, i, j)$	(37)	
$Q_n^{cond} = U_n^{cond} A_n^{cond} LMTD_n^{cond}$	$\forall n \in COND(n, i, j)$	(38)	
$m_i = m_j + m_k$	$\forall i, j, k \in SP(i, j, k)$	(39)	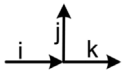
$T_i = T_j = T_k$	$\forall i, j, k \in SP(i, j, k)$	(40)	
$m_i + m_j = m_k$	$\forall i, j, k \in MX(i, j, k)$	(41)	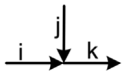
$mH_i + mH_j = mH_k$	$\forall i, j, k \in MX(i, j, k)$	(42)	
$m_i + m_j = m_k$	$\forall n, i, j, k \in DEA(n, i, j, k)$	(43)	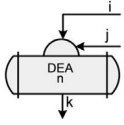
$mH_i + mH_j = mH_k$	$\forall n, i, j, k \in DEA(n, i, j, k)$	(44)	
$T_k = T_k^{sat}$	$\forall n, k \in DEA(n, i, j, k)$	(45)	

3.2.2.3. Selection of the number of economizers and superheaters in each section of the HRSG and in each pressure level. According to Fig. 1, it is clear that in a dual pressure heat recovery steam generator at least one economizer and one superheater must be selected in each pressure level. Precisely, in the low pressure level, the economizers EC1 and/or EC2 and superheaters SH1 and/or SH2 and/or SH3 and/or SH4 must be selected. In a similar way, in the high pressure level, the economizers EC3 and/or EC4 and/or EC5 and/or EC6 and superheaters SH5 and/or SH6 must also be selected. As a first approximation, it is considered that only one economizer and one superheater can be selected in each pressure level.

Thus, the following constraints are imposed for the low pressure level:

$$x_1^{ec} + x_2^{ec} = 1 \tag{52}$$

$$x_1^{sh} + x_2^{sh} + x_3^{sh} + x_4^{sh} = 1 \tag{53}$$

Similarly, the following constraints are considered for the high pressure level:

$$x_3^{ec} + x_4^{ec} + x_5^{ec} + x_6^{ec} = 1 \tag{54}$$

$$x_5^{sh} + x_6^{sh} = 1 \tag{55}$$

3.2.2.4. Avoiding the selection of more than one heat exchangers in each section of the HRSG.

$$x_n^{sh} + x_{n'}^{sh} \leq 1 \quad \forall n, n', p, q \in SHSH(n, n', p, q) \tag{56}$$

$$x_n^{ec} + x_{n'}^{sh} \leq 1 \quad \forall n, n', p, q \in SHEC(n, n', p, q) \tag{57}$$

$$x_n^{ec} + x_{n'}^{ec} \leq 1 \quad \forall n, n', p, q \in ECEC(n, n', p, q) \tag{58}$$

3.2.2.5. Constraints included to avoid repetitive optimal solutions. Usually, when a superstructure is proposed in order to include many alternative configurations repetitive solutions can be obtained. That is, different optimal solutions may imply the same optimal configuration. For a more clear visualization of this, let us to consider the following three potential situations that may be appeared when the superheaters SH1 and SH2 and economizers EC5 and EC6 are considered (Fig. 7(a)):

a) No heat exchanger is selected. In this situation, no repetitive solutions are possible and the Eqs. (52)–(58) are enough to remove these heat exchangers.
b) Two heat exchangers are selected (one superheater: SH1 or SH2 and one economizer: EC5 or EC6). In this situation, two optimal configurations may be selected which are illustrated in Fig. 7(b) and (c) and therefore no repetitive solutions are possible. As in the previous case, the Eqs. (52)–(58) are enough to model these alternative configurations.
c) Only one heat exchanger is selected (SH1 or SH2 or EC5 or EC6). In this situation, four configurations may be selected which are illustrated from Fig. 7(d) to (g). In contrast to the previous cases, repetitive solutions are observed. For instance, from a practical point of view, the configuration shown in Fig. 7(d) (solution in which $x_1^{sh} = 1$; $x_2^{sh} = x_5^{ec} = x_6^{ec} = 0$) is exactly the same as the configuration shown in Fig. 7(e) (solution in which $x_2^{sh} = 1$; $x_1^{sh} = x_5^{ec} = x_6^{ec} = 0$). Also, the configurations illustrated in Fig. 7(f) and (g) are equivalent and the same configuration can be expressed by two different set of numerical values ($x_5^{ec} = 1$; $x_1^{sh} = x_2^{sh} = x_6^{ec} = 0$ and $x_6^{ec} = 1$; $x_1^{sh} = x_2^{sh} = x_5^{ec} = 0$).

The repetitive solutions can be overcome with the inclusion of additional constraints. The constraints will be proposed in such a way as to give the possibility to select the configurations shown in Fig. 7(d) and (f) instead of the configurations shown in Fig. 7(e) and (g). This consideration is imposed by the following linear constraints which are expressed in terms of their corresponding binary variables. Precisely, Eqs. (59) and (60) exclude the configurations shown in Fig. 7(e) and (g), respectively.

$$x_1^{sh} + x_5^{ec} + 1 - x_2^{sh} \geq 1 \tag{59}$$

$$x_1^{sh} + x_5^{ec} + 1 - x_6^{ec} \geq 1 \tag{60}$$

If $x_1^{sh} = x_5^{ec} = 0$, by Eq. (59) $x_2^{sh} = 0$ and by Eq. (60) $x_6^{ec} = 0$ and the configurations shown in Fig. 7(e) and (g) are excluded.

Here, it is important to notice that other repetitive solutions can be observed for the ECEC section (EC1/EC2/EC3/EC4) as well as for the SHSH section (SH3/SH4/SH5/SH6). Then, by following the same reasoning as the previous case, Eqs. (61) and (62) are proposed for ECEC section, and Eqs. (63) and (64) for the SHSH section.

$$x_1^{ec} + x_3^{ec} + 1 - x_2^{ec} \geq 1 \tag{61}$$

$$x_1^{ec} + x_3^{ec} + 1 - x_4^{ec} \geq 1 \tag{62}$$

$$x_3^{sh} + x_5^{sh} + 1 - x_4^{sh} \geq 1 \tag{63}$$

$$x_3^{sh} + x_5^{sh} + 1 - x_6^{sh} \geq 1 \tag{64}$$

3.2.3. Physicochemical properties

Finally, the model includes the following correlations to compute the stream thermodynamic properties. As shown, three sets are defined that identify the state of the working fluid (water) in each point of the process unit. For instance, the sets denoted by LIQ, VAP and TIT refer, respectively, to liquid state, steam saturated and reheated steam) and steam quality. Each one of the set is indexed on "i" which identifies the process stream (working fluid).

For the streams that are in the liquid state, the following constraints apply:

$$T_i \leq T_i^{sat} \quad \forall i \in LIQ(i) \tag{65}$$

$$H_i = f_L(P_i, T_i) \quad \forall i \in LIQ(i) \tag{66}$$

$$S_i = f_L(P_i, T_i) \quad \forall i \in LIQ(i) \tag{67}$$

For the streams that are in the vapor state, the following constraints apply the following constraints:

$$T_i \geq T_i^{sat} \quad \forall i \in VAP(i) \tag{68}$$

$$H_i = f_V(P_i, T_i) \quad \forall i \in VAP(i) \tag{69}$$

$$S_i = f_V(P_i, T_i) \quad \forall i \in VAP(i) \tag{70}$$

For the streams that are composed by a mixture of steam and liquid water, that is wet steam with a steam quality xi, the following constraints are used:

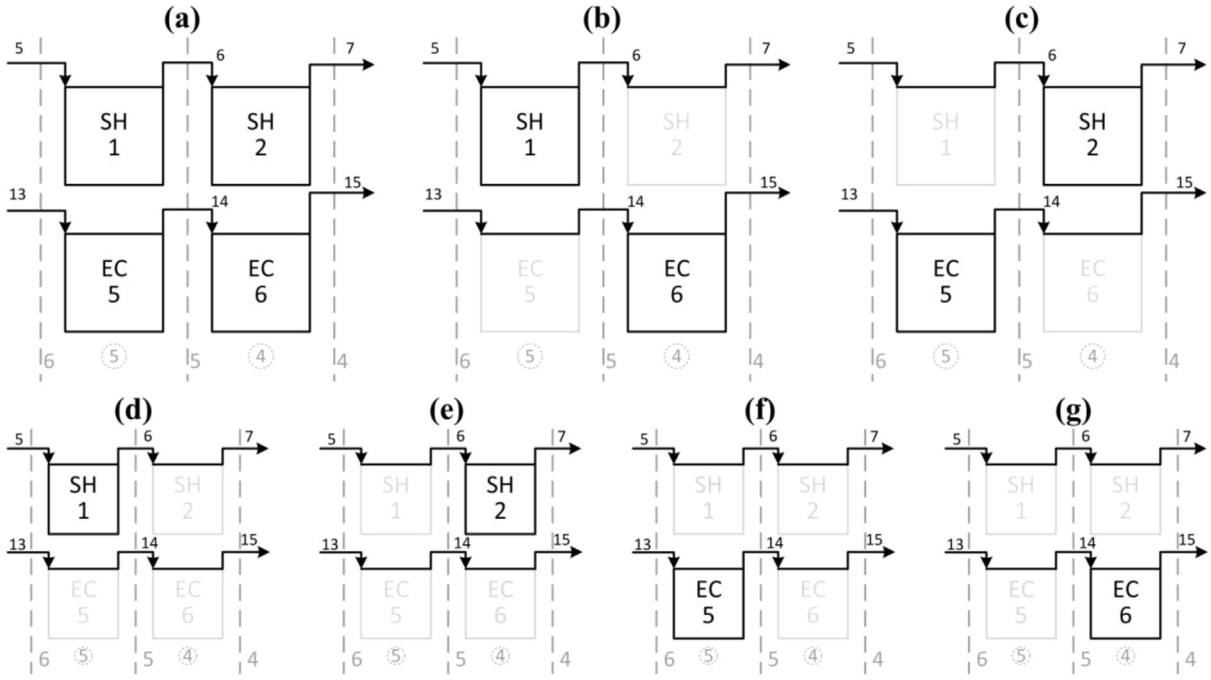

Fig. 7. Possible repetitive optimal solutions.

$$T_i = T_i^{sat} \quad \forall i \in TIT(i) \tag{71}$$

$$H_i = x_i f_V(P_i, T_i) + (1 - x_i) f_L(P_i, T_i) \quad \forall i \in TIT(i) \tag{72}$$

$$S_i = x_i f_V(P_i, T_i) + (1 - x_i) f_L(P_i, T_i) \quad \forall i \in TIT(i) \tag{73}$$

$$T_i = T_i^{sat} \quad \forall i \ SAT(i) \tag{74}$$

Finally, the total energy of the water stream is calculated as follows:

$$mH_i = m_i H_i \quad \forall i \in MH(i) \tag{75}$$

The dependence of the enthalpy with the temperature and the total energy of the gas stream are given by the Eqs. (76) and (77):

$$H_p = f_G(T_p) \quad \forall p \in GAS(p) \tag{76}$$

$$mH_p = m_p H_p \quad \forall p \in GAS(p) \tag{77}$$

Also, the model includes the following two inequality constraints related to the minimum pinch point and minimum heat transfer temperature difference

$$T_q - T_i^{sat} \geq Pinch \quad \forall q, i \in EV(n, i, j, p, q) \tag{78}$$

$$T_p - T_i \geq \Delta T_{\min} \quad \forall p, i \in DT(p, i) \tag{79}$$

According to these constraints, the pinch point refers to the temperature difference between the gas that leaves the evaporator and saturation temperature of the working fluid (water) while the minimum heat transfer temperature difference in each heat exchanger is defined as the difference between the outlet (inlet) gas temperature and the inlet (outlet) water temperature.

Finally, the following inequality constraint is also imposed on the exhaust gas temperature at the HRSG outlet in order to prevent condensation of acid components.

$$T_9 \geq 393K \tag{80}$$

3.2.4. Objective functions

In order to evaluate the model's strength, it has preferred to use simple objectives based on the variables that are included in the mass and energy balances. As a first step in the modeling task, the idea was to keep the size of the model as small as possible (simple objective function, constant U-values, among others). Exergy efficiency and/or cost will be further considered as objective functions. This will require to include the corresponding exergy balances and/or cost model resulting in a more complex model. In this sense, the model presented in this paper may be considered to be part of the solution strategy for optimization such objective functions. In fact, a solution strategy may be easily implemented in GAMS where, in a first step, the current model is solved and then the solution is used in a second step to solve the complete model (current model plus all constraints related to the calculations of the exergy losses in the process-units or the total annual cost).

Consequently, based on the above, the proposed model has been solved for two single objective functions. One of the objective function is the minimization of the total heat transfer area computed by Eq. (81) and the other one is the maximization of the total net power computed by Eq. (82).

$$THTA = \sum_{n=1}^{6} A_n^{ec} + \sum_{n=1}^{3} A_n^{ev} + \sum_{n=1}^{6} A_n^{sh} + A_1^{cond} \tag{81}$$

$$TNP = W_1^{st} + W_1^{ste} - \sum_{n=1}^{4} W_n^{pump} \tag{82}$$

The proposed mathematical model involves 277 continuous variables, 14 binary variables and 383 constraints (equality and inequality constraints). In addition, lower and upper bounds in some variables are considered in order to obtain feasible designs. It was implemented in GAMS 23.9.5 (General Algebraic Modeling

System) which is specifically a high-level modelling system for solving large-scale numerical programming problems involving both discrete and continuous variables. GAMS has been successfully applied in several other areas allowing to find novel and improved processes [45–47]. DICOPT (DIscrete and Continuous OPTimizer) was used as MINLP solver [48], CPLEX for MIP (mixed integer problem) solver [49], and CONOPT, which is based on the generalized reduced gradient algorithm, was used as NLP (non-linear problem) solver [50]. It should be addressed that global optimal solutions cannot be guaranteed due to the non-convex constraints involved in the bilinear terms related to the energy and mass balances, among others.

The used optimization methodology consists of a sequence of non-linear (NLP) sub-problems and MILP (mixed integer lineal) master problems. The NLP sub-problem provides an upper bound for the primal problem while the MILP problem provides a lower bound of the primal problem. Then, both NLP and MILP sub-problems are solved in a cycle of iterations until the up-date relative gap of those bounds satisfy the tolerance criteria.

4. Discussion of results

The numerical values of the model parameters, lower and upper bounds used for all of the optimizations are listed in Tables 2 and 3, respectively. For comparison purposes, the bounds for high and low pressure have been taken from Zhang et al. [36]. The values for the other bounds were only to facilitate the model convergence. For instance, the upper bound in the heat transfer area and mass flow-rate were included to avoid potential unbounded values in some of the iterations. Finally, it should be mentioned that the reference case data taken from Zhang et al. [36] is numerical.

4.1. Verification model

In order to verify the proposed model, model outputs are compared with data from Ref. [37] which correspond to a case of existing HRSG configuration. Therefore, various optimization variables in the proposed MINLP model are fixed at the same values as in Ref. [37] for recreating the reported solution. Thus, the proposed MINLP model was used as a simulator rather than an optimizer. Table 4 compares the results in terms of the stack gas temperature, the total heat transferred in the HRSG, and the total power production in the steam turbines. As shown, the simulated MINLP solution agrees satisfactorily with the data reported in Ref. [37].

Table 2
Values of model parameters used in all case studies.

Flue gas specification	Unit	Value	Source
Gas turbine exhaust mass flow	kg/s	141.9	[36]
Gas turbine exhaust temperature	K	894.1	[36]
Composition			[36]
H_2O		0.08303	
CO_2		0.03715	
N_2		0.74463	
O_2		0.12623	
Minimum exhaust gas temperature	K	393.1	[36]
Process units			
Economizer overall heat transfer coefficient	W/(m^2 K)	42.6	[37]
Evaporator overall heat transfer coefficient	W/(m^2 K)	43.7	[37]
Superheater overall heat transfer coefficient	W/(m^2 K)	50	[37]
Minimum pinch point	K	15	[36]
Approach point	K	10	[36]
Minimum heat transfer temperature difference	K	15	[36]
Deaerator pressure	Bar	0.20	[this work]
Condenser pressure	Bar	0.04	[this work]
Isentropic efficiencies of steam turbines	Unitless	0.80	[this work]
Isentropic efficiencies of pumps	Unitless	0.80	[this work]

Table 3
Lower and upper bounds for optimization variables used in all case studies.

Variable		Lower bound	Upper bound	Source
High pressure	Bar	70	80	[36]
Low pressure	Bar	6	7	[36]
Temperature	K	302.1	950	[36]
Mass flow-rate	kg/s	0	100	[this work]
Heat transfer area	m^2	0	1 10^6	[this work]

4.2. Optimization results

Once the proposed mode was successfully verified, it was used to solve the optimization problem stated in the Section 2 but for RC (HRSG configuration reported by Zhang et al. [36]). Therefore, various optimization variables in the proposed MINLP model were fixed for recreating the configuration obtained by Zhang et al. [36]. Precisely, the flow-rate in stream#27 and the high and low pressures were set at 23.6 kg/sec, 70 and 6 bar, respectively, and also the outlet temperatures of the working fluid at 671.0 and 864.0 K. After that, the model is solved considering the possibility to split the stream #2 and therefore to use the pump #1 in order to determine its optimal layout, size and operating conditions that maximize the total power production for the same total heat transfer area used in RC (OD1). Also, a third optimization problem with the objective to minimize the total heat transfer area for the same power production obtained in the RC (OD2) has been also solved. Then, the three optimal designs are compared in terms of the obtained configuration, total heat transfer area, total net power generation and operating conditions.

Tables 5 and 6 summarize the optimal values that correspond to the heat transfer area, heat load in each process-unit as well as the power produced in each steam turbine and the power required by the pumps for each optimization design (RC, OD1 and OD2) and Figs. 8–10 include the corresponding optimal values of flow-rate, temperature and pressure of the all of the streams. In addition, temperature-enthalpy rate diagrams for each one of the optimal solutions are presented in Figs. 11–13 in order to illustrate the optimization results.

One of the qualitative results reveals that the selection of the Pump #1 does not depend on the objective function used for optimization. In both OD1 and OD2, the Pump #1 has been selected, affecting in different ways the optimal operating conditions.

As it can be seen in Table 5, the TNP obtained by OD1 is higher compared to RC [36] in about 8% when a same THTA is involved in both cases. One of the main differences between both designs is the configuration of the HRSG. By comparing the configurations of HRSG in RC (Fig. 8) and OD1 (Fig. 9), it is possible to observe that despite that the THTA available in the entire process and the number of heat exchangers are the same in both cases they are interconnected in different way. Precisely, in OD1 the stream #2 that leaves the economizer EC1 is split into stream #3 and #19 compared to RC where no streams are split. Also it is interesting to observe that the number of pumps required in both designs is the same (3 pumps) but they are placed in different zones of the HRSG which is also another difference between OD1 and RC. In the RC (Fig. 8) two pumps #2 and #3 are placed after the deareator to flow respectively the stream #29 into the EC1 which works in the zone

Table 4
Model verification.

Parameter	Unit	This work	Franco and Giannini (2006) [37]
Stack gas temperature	K	398.5	398.2
Total heat transferred in HRSG	MW	189.4	189.6
Total power generated in steam turbines	MW	58.1	58.2
Gas turbine exhaust mass flow	kg/s	445.4[a]	
Gas turbine exhaust temperature	K	778.2[a]	
Condenser and deaerator pressure	Bar	0.18[a]	
High pressure steam mass flow-rate	kg/s	48.3[a]	
Low pressure steam mass flow-rate	kg/s	13.2[a]	
High pressure	Bar	53.8[a]	
Low pressure	Bar	5.4[a]	
High pressure steam temperature	K	763.2[a]	
Low pressure steam temperature	K	546.2[a]	

[a] Fixed values.

Table 5
Summary of the optimal total heat transfer area and net power for the three optimal designs.

	Total heat transfer area (m^2)	Total net power (kW)	Total CPU time (sec)	Number of iterations
RC [36]	20417.8	24419.3	0.421	93
OD1	20417.8	26388.4	3.962	1243
OD2	15557.9	24419.3	4.336	1192

of the low pressure and the stream #28 into the EC5 which works in the zone of the high pressure. In contrast to this, in the OD1, only one pump is located after the deareator (pump #3) which is used to flow the stream #29 into the EC1. As shown, the stream #2 is then split into the following two streams: a) stream #3 which flows to the EV1 located in the low pressure level and b) stream #19 which passes through the pump #1, increases its pressure and flows into the economizer EC5 located in the high pressure level. The inclusion of the Pump #1 in OD1 allowed to increase the pressure from 7 to 80 bar compared to the RC [36] where the high pressure is about 70 bar. In addition, the steam flow-rate in EC5 and therefore in the steam turbine ST1 has been also increased by the use of the pump #1 compared to the RC (19.01 vs 13.48 kg/sec), resulting in a higher generation of TNP. As indicated in Table 6, the total work required by pumps in OD1is slightly higher than that required in RC, 169.6 vs 102.0 kW, indicating that the inclusion of the pump #1 does not affect the total work required by pumps significantly. On the other hand and as expected, the TNP produced in the steam turbines in OD1 is much more higher compared to RC (26558.1 versus 24521.4 kW) resulting in a higher net power production for a same THTA (20417.8 m^2). In this regards, it is also interesting to see that, although the power production in STe_1 in RC is higher than in OD1 (16634.1 vs 15773.0 kW), the power production in W_1^{st} in RC [36] is much less than in OD1 (7887.2 vs 10785.0 kW).

Table 6
Optimal solutions obtained for different configurations.

	Process unit	RC [36]	OD1	OD2
Heat transfer area (m^2)	EC LP	1769.5	3048.6	2048.8
	EV LP	8724.6	3016.8	2074.7
	SH LP	432.0	289.2	236.4
	EC HP	1775.5	3371.0	2413.9
	EV HP	3047.3	5474.0	4389.2
	SH HP	2198.2	2861.0	2180.4
	COND	2470.4	2356.9	2214.3
		20417.8	**20417.7**	**15557.9**
LMTD (K)	EC LP	50.6	72.4	101.7
	EV LP	56.7	70.4	97.9
	SH LP	240.2	93.2	112.3
	EC HP	170.6	79.9	103.5
	EV HP	157.7	118.9	140.6
	SH HP	105.1	110.3	129.4
Heat load in HRSG (kW)	EC LP	3816.8	9409.0	8877.1
	EV LP	21644.2	9291.9	8877.3
	SH LP	5189.4	1349.0	1327.4
	EC HP	12907.8	11485.7	10646.6
	EV HP	21008.1	28446.7	26971.1
	SH HP	11551.7	15782.7	14107.4
	COND	51680.9	49305.8	46322.6
		127799.1	**125071.22**	**117129.8**
Power (kW)	W_1^{st}	7887.2	10785.0	9836.7
	W_1^{ste}	16634.1	15773.0	14738.6
		24521.441	**26558.13**	**24575.3**
	W_1^{pump}	0	152.1	139.2
	W_2^{pump}	95.7	0	0
	W_3^{pump}	5.9	16.1	15.2
	W_4^{pump}	0.3	1.3	1.4
		102.0	**169.6**	**156.0**
Total Net Power (kW)		**24419.3**	**26388.4**	**24419.3**

A third optimization problem has been also solved (OD2) but now considering the minimizing of THTA to produce the same net power production obtained in the RC. As shown in Fig. 10, the optimal arrangement is similar to that obtained in Fig. 9 (OD1) and therefore is different to that involved in Fig. 8 (RC). For the same net power production of 24419.3 MW, the THTA required in OD2 is significantly lower than that required in RC [36] in about 24% (15557.9 versus 20417.8 m^2). As shown in Table 6, the optimal placement of the pumps leads to increase both the power consumptions by pumps and to increase the power production by steam turbines in order to guarantee the fixed net power production. It is interesting to observe that the heat transfer area required by each heat exchanger for OD2 is lower than that required in OD1. This is because of two reasons. The first is that the heat loads involved in the units for OD2 are lower than in OD1. The second is that the differences of temperature in the cold and hot sides of the units which affect the corresponding driving forces in OD2 are higher than in OD1, as it can be seen by comparing the T-H diagrams for OD2 (Fig. 13) and OD1 (Fig. 12). For instance, 2048.8 m^2 is required in the EC LP OD2 for a heat load of 8877.1 kW and a driving force of 101.7 K, in comparison to that involved in OD1 where is required 3048.6 m^2 for a heat load of 9409.0 kW with a driving force of 72.4 K. However, a different distribution of heat transfer areas can be observed between OD2 and RC [36]. Although the heat

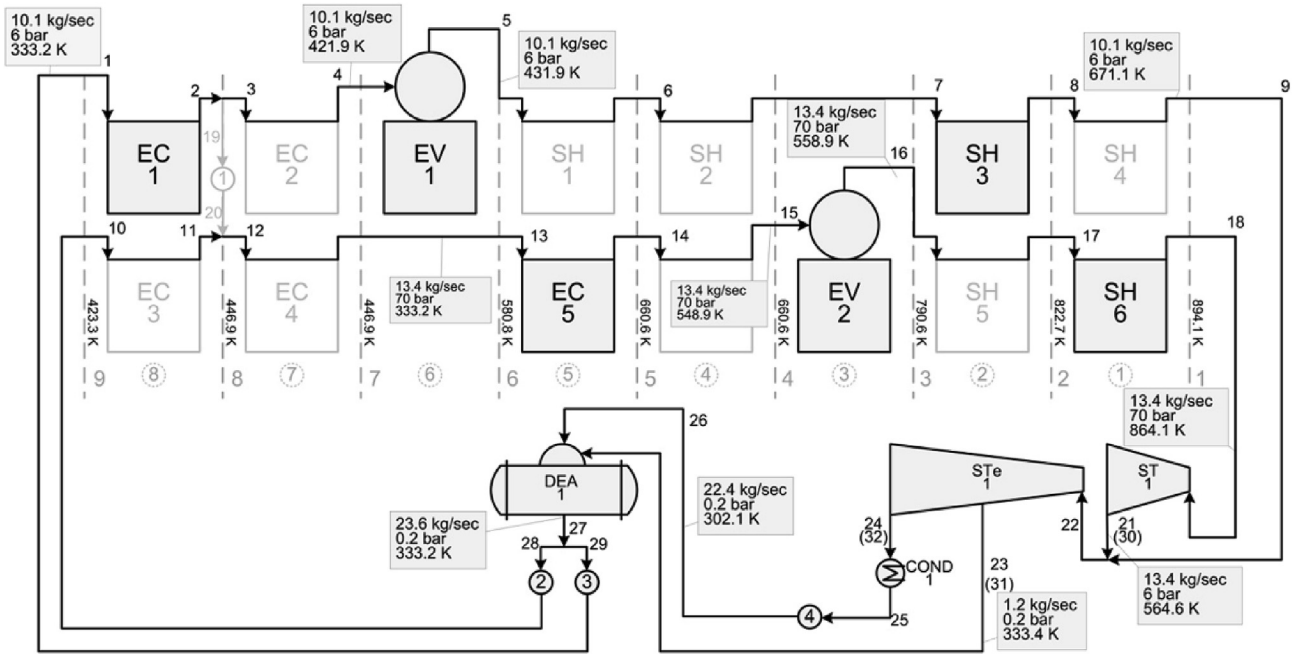

Fig. 8. Optimal solution obtained for the reference case [36].

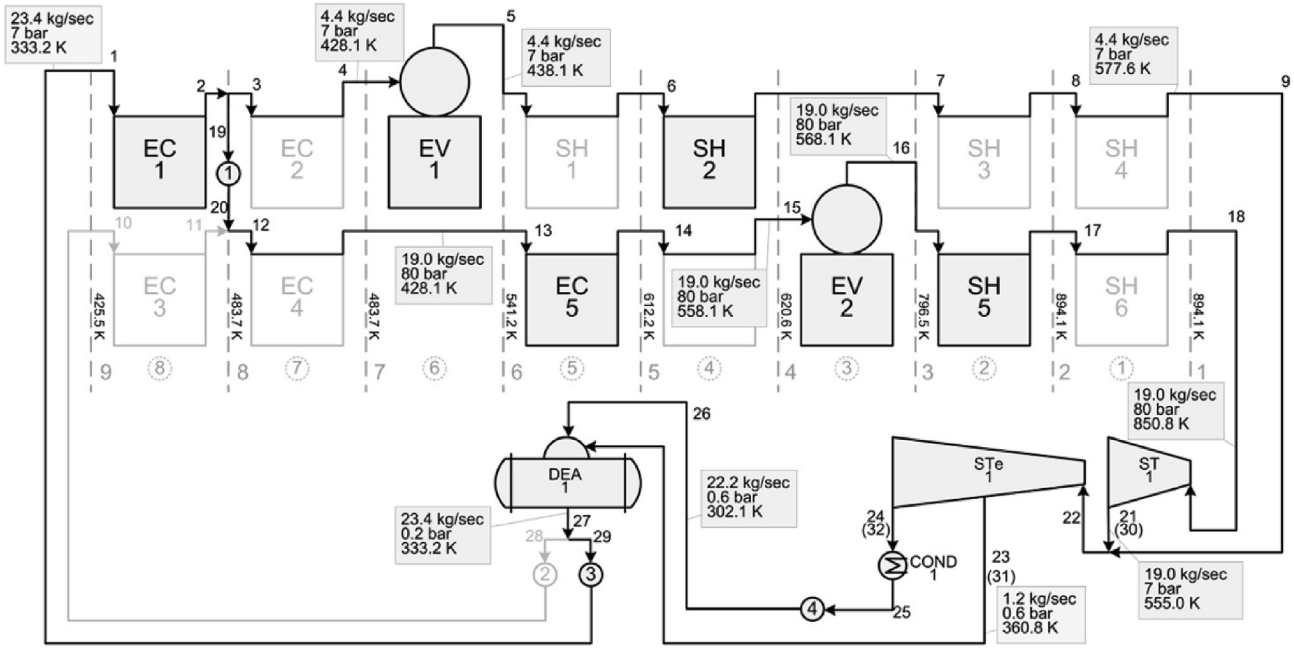

Fig. 9. Optimal solution obtained for the maximization of the total net power for a given total heat transfer area.

transfer area required in EC LP, EC HP and EV HP in OD2 are higher than that required in RC, the heat transfer area required in EV LP is considerably much less than in RC (8724.6 vs 2074.7 m^2) resulting in a lower THTA. The area in SH HP and COND in OD2 are also lower than in RC but not as much as the EV LP. Finally, it is interesting to see in the T-H diagrams for RC in Fig. 11 that T_2 tends to T_7 in EV1 increasing significantly the corresponding heat transfer areas. However, the minimization of the THTA (total heat transfer area) leads to increase the driving force by increasing the difference between T_2 and T_7 as it can be clearly seen in Fig. 13, in contrast to that observed in Fig. 11.

Finally, it is interesting to present the computational cost required to solve each one of the optimization problems. As shown in Table 5, RC [36] requires less total CPU time and iterations because the configuration is fixed and therefore no discrete decisions are involved.

4.3. Trade-offs between total heat transfer area and total net power

Finally, the comparison of results between the current configuration and the reference configuration [36] can be also extended by maximizing the total net power for a wide range of total heat

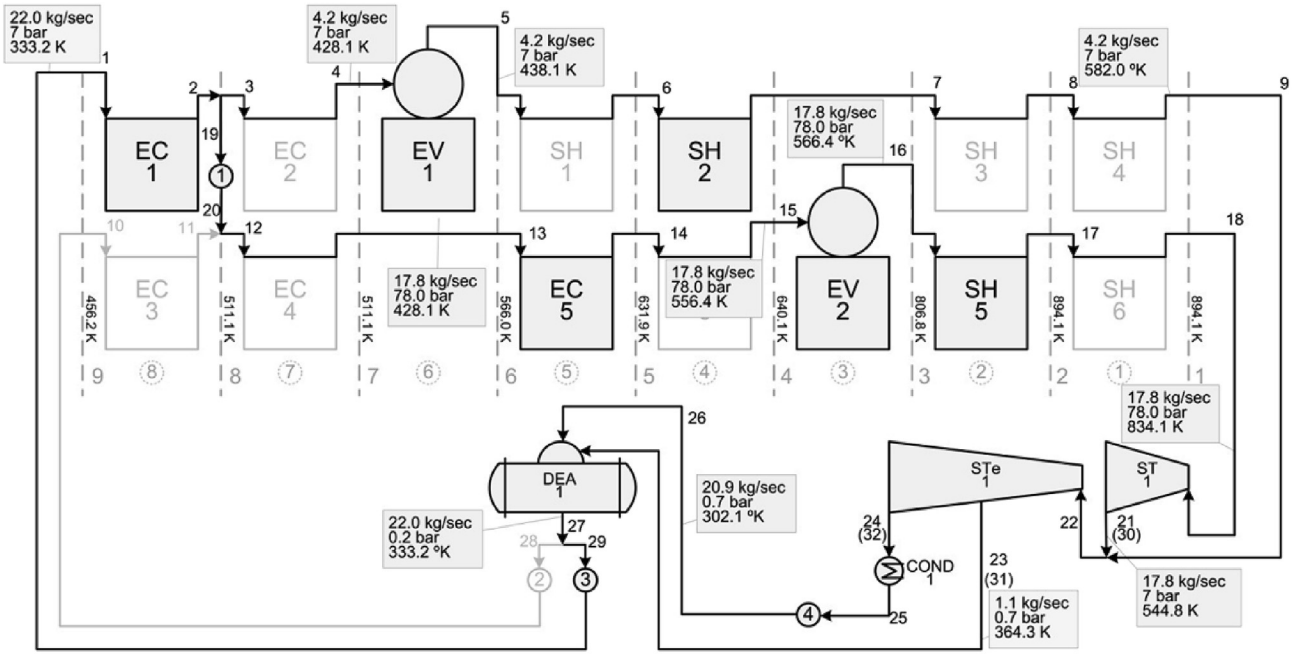

Fig. 10. Optimal solution obtained for the minimization of the total heat transfer area for a given total net power production.

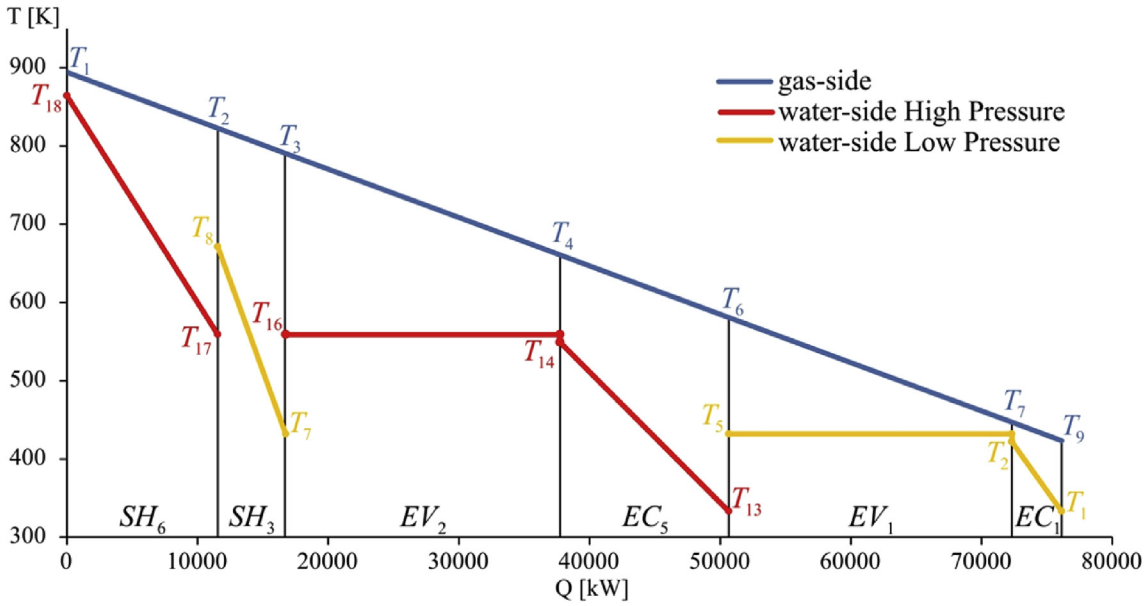

Fig. 11. Temperature-enthalpy rate diagram obtained for the reference case [36].

transfer area. In order to obtain the optimal solutions for the RC, the flow-rate of the stream#27 has been considered as an optimization variable instead of a fixed value of 23.6 kg/sec which has been used to recreate the Zhang's solution in the Section 4. In addition, the high and low pressures and inlet and outlet temperatures at the HRSG have been also considered as optimization variables. As it can be clearly seen, the current optimal configuration produces more total net power compared to the reference case. It can be seen that the TNP obtained by the current model increases from 24419.3 kW at 15557.9 m^2 to 29015.3 kW at 36682.7 m^2 and then it remains constant because some of the inequality constraints included to prevent temperature cross-overs become to be equality constraints, indicating that temperature differences tend to zero. A similar behavior can be also observed for the RC, but the TNP reaches a constant value of 26806.3 kW from 26435.63 m^2 (Fig. 14).

4.4. Assessment of the validity of the main modeling assumptions

4.4.1. Chen's approximation used to compute heat transfer areas

In order to assess the validity of modeling assumption about the use of Chen's approximation instead of LMTD method, the MINLP model was also solved for LMTD method using as initialization the solution obtained for Chen's approximation. Table 7 compares the results in terms of the driving force and heat transfer area of each heat exchanger. As shown, the comparison reveals that both solutions are almost similar. Chen's approximation is still preferred

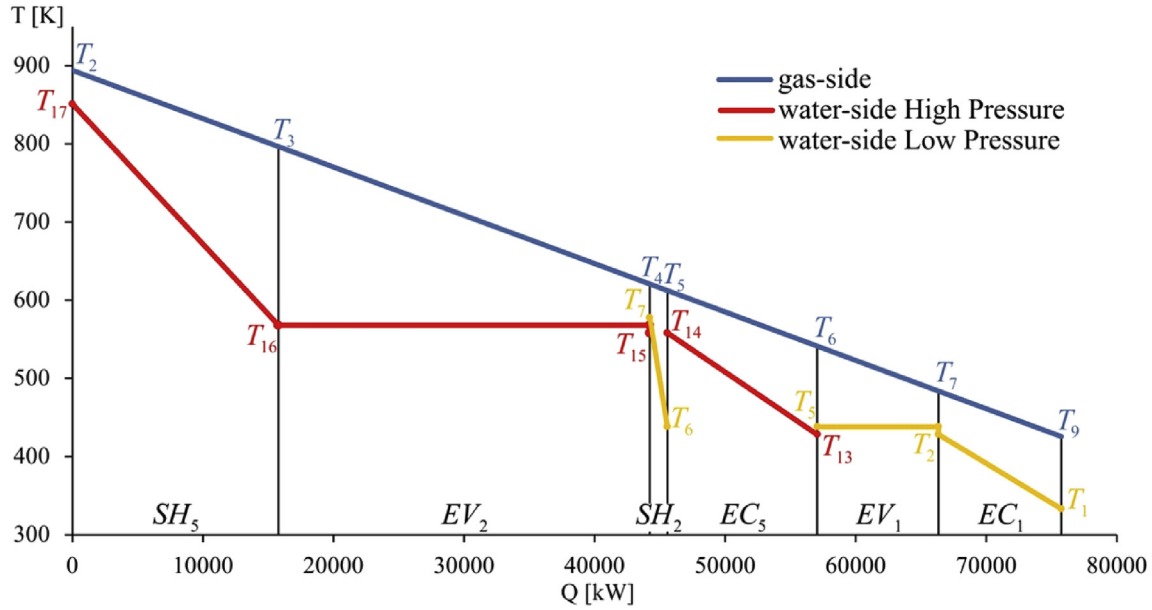

Fig. 12. Temperature-enthalpy rate diagram obtained for the maximization of the total power for a given total heat transfer area.

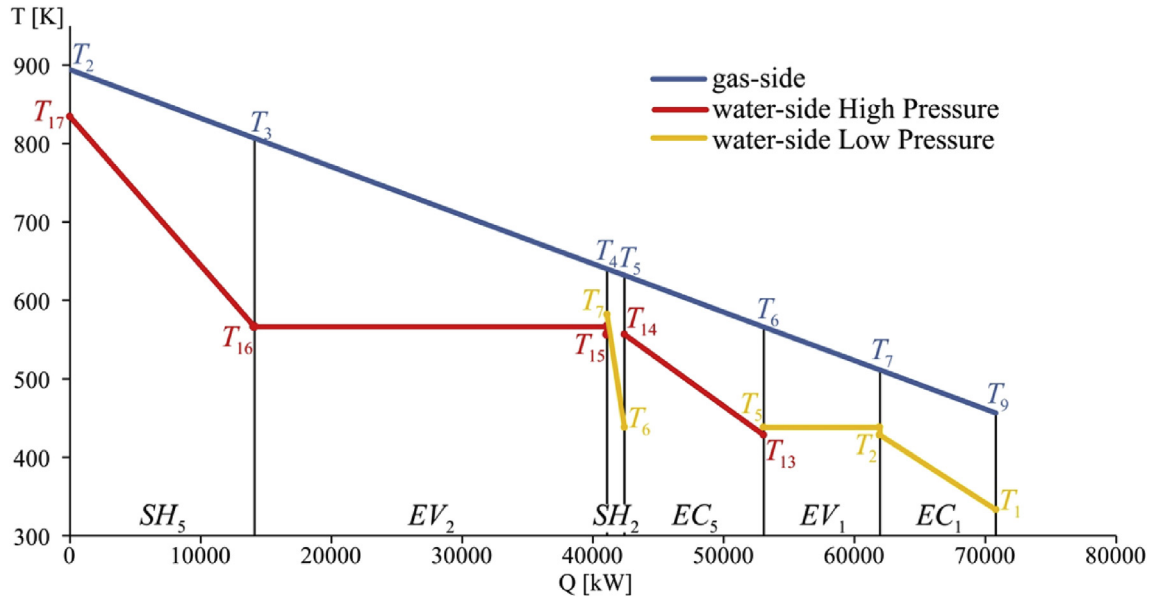

Fig. 13. Temperature-enthalpy rate diagram obtained for the minimization of the total heat transfer area for a given total power production.

than the LMTD method in order to avoid convergence problems when the heat exchangers need to be removed.

4.4.2. Pumping work calculation assuming water as an incompressible fluid

In order to verify if the approximation of incompressible fluid is suitable for the pressure levels considered at states (2) and (20), the pumping work was computed assuming both cases: compressible and incompressible conditions. The comparison of results obtained for RC [36], OD1 and OD2 revealed that the assumption of incompressibility condition to compute the pumping work in Pump 1 does not affect the optimization results. For instance, the pumping works and outlet temperature computed under both conditions for OD1 differ only in about 0.1 kW and 0.8 °C, respectively.

5. Conclusions

This paper presents a discrete and continuous mathematical model for the optimal synthesis and design of dual pressure heat recovery steam generators coupled to two steam turbines. The MINLP proposed model determines how the heat exchangers (economizers, evaporators and superheaters) in the HRSG should be connected in order to optimize a single objective function proposed by the user. In this paper, the following two objective functions have been proposed: a) the maximization of the total net power for a given total heat transfer area (OD1) and b) the minimization of the total heat transfer area for a given total net power (OD2). The optimal configuration is selected from a superstructure of alternative arrangements, and the operating conditions and size of each process unit are determined simultaneously.

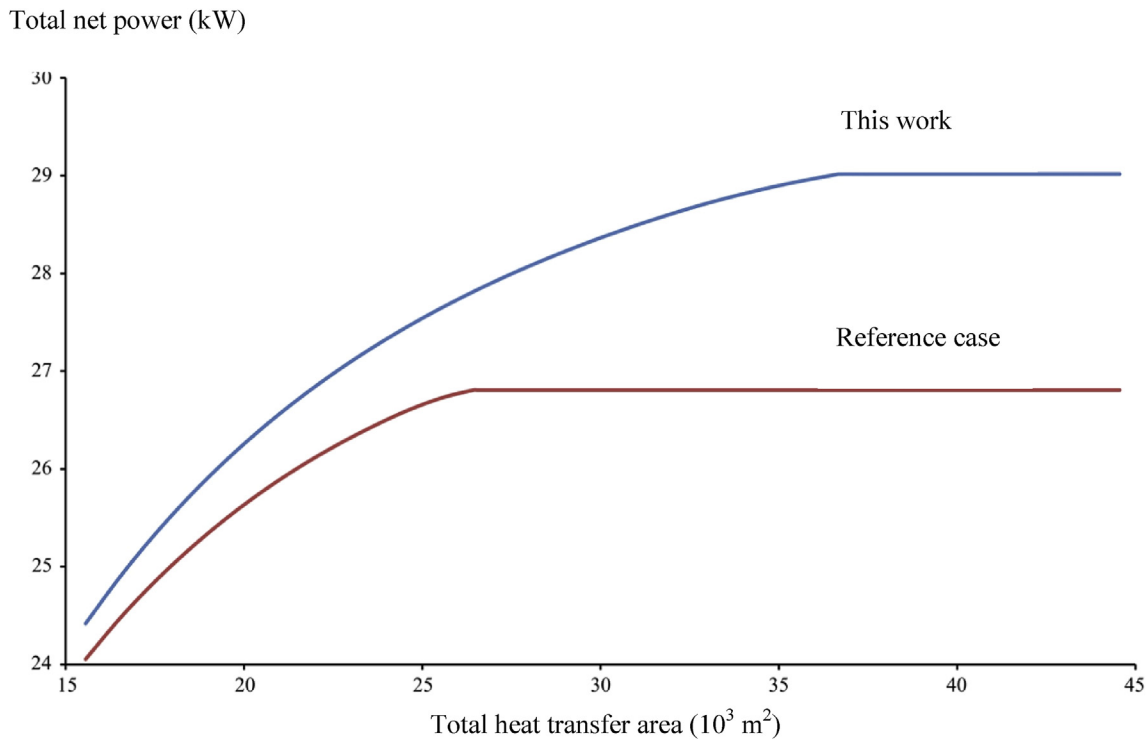

Fig. 14. Optimal values of total net power vs. total heat transfer area.

Table 7
Comparison of results obtained by the LMTD method and Chen's approximation.

	Driving force (°K)		Heat transfer area (m^2)	
	LMTD method	Chen's approximation	LMTD method	Chen's approximation
EC LP	72.4	72.4	3048.3	3048.6
EV LP	70.5	70.4	3015.0	3016.8
SH LP	93.7	93.2	287.9	289.2
EC HP	80.0	79.9	3369.7	3371.1
EV HP	119.5	118.9	5443.7	5474.1
SH HP	111.2	110.3	2836.1	2860.9
Total			**18000.7**	**18060.7**

The optimization results obtained in OD1 and OD2 have been discussed in detail and they were compared with a reference case reported by other authors [36]. Based on the optimal solutions, one of the qualitative results reveals that a similar optimal configuration was obtained in OD1 and OD2 which is more efficient than that obtained in the RC. Precisely, the proposed superstructure permitted a better allocation of heat exchangers and pumps in the HRSG compared with the RC which allow to increase the power production in about 8.00%,from 24419.4 (OD1) to 26380.5 kW (RC), and to decrease the total heat transfer area in about 24.00%, from 20417.8 (RC) to 15557.9 m^2 (OD2).

The proposed model is being extended to include the following points: a) three pressure levels, b) gas turbines available in the market, c) detailed models of each heat exchanger in order to include the pressure drop in the cold and hot sides, the variability of the global heat transfer coefficients with velocity and temperature, number and arrangement of tubes: square or triangular pitch and c) a detailed cost model in order to minimize the total annual cost. These considerations will increase the number of combinations, and it may still be possible to find novel designs with substantially improved efficiency. In addition, the proposed model will be also complemented with other models developed previously by the authors. In fact, mathematical models of thermal desalination systems and/or CO_2 capture plants will be coupled into the model presented in this paper in order to optimize the synthesis and design of the entire process.

Acknowledgments

The following two organizations are gratefully acknowledged for their financial support: Consejo Nacional de Investigaciones Científicas y Técnicas (CONICET) and the Universidad Tecnologica Nacional Facultad Regional Rosario (UTN-FRRo, Argentina).

References

[1] Tajik Mansouri M, Ahmadi P, Ganjeh Kaviri A, Jaafar MNM. Exergetic and economic evaluation of the effect of HRSG configurations on the performance of combined cycle power plants. Energy Convers Manag 2012;58:47–58. http://dx.doi.org/10.1016/j.enconman.2011.12.020.
[2] Sanjay. Investigation of effect of variation of cycle parameters on thermodynamic performance of gas-steam combined cycle. Energy 2011;36:157–67. http://dx.doi.org/10.1016/j.energy.2010.10.058.
[3] Regulagadda P, Dincer I, Naterer GF. Exergy analysis of a thermal power plant with measured boiler and turbine losses. Appl Therm Eng 2010;30:970–6. http://dx.doi.org/10.1016/j.applthermaleng.2010.01.008.

[4] Tsatsaronis G, Park M-H. On avoidable and unavoidable exergy destructions and investment costs in thermal systems. Energy Convers Manag 2002;43:1259–70. http://dx.doi.org/10.1016/S0196-8904(02)00012-2.
[5] Morosuk T, Tsatsaronis G. Comparative evaluation of LNG – based cogeneration systems using advanced exergetic analysis. Energy 2011;36:3771–8. http://dx.doi.org/10.1016/j.energy.2010.07.035.
[6] Tsatsaronis G, Morosuk T. Advanced exergetic analysis of a novel system for generating electricity and vaporizing liquefied natural gas. Energy 2010;35:820–9. http://dx.doi.org/10.1016/j.energy.2009.08.019.
[7] Tsatsaronis G. Strengths and limitations of exergy analysis. In: Bejan A, Mamut E, editors. Thermodyn. optim. complex energy syst. Netherlands: Springer; 1999. p. 93–100.
[8] Taillon J, Blanchard RE. Exergy efficiency graphs for thermal power plants. Energy 2015;88:57–66.
[9] Arriola-Medellín A, Manzanares-Papayanopoulos E, Romo-Millares C. Diagnosis and redesign of power plants using combined pinch and exergy analysis. Energy 2014;72:643–51. http://dx.doi.org/10.1016/j.energy.2014.05.090.
[10] Liao C, Ertesvåg IS, Zhao J. Energetic and exergetic efficiencies of coal-fired CHP (combined heat and power) plants used in district heating systems of China. Energy 2013;57:671–81. http://dx.doi.org/10.1016/j.energy.2013.05.055.
[11] Khaliq A, Dincer I. Energetic and exergetic performance analyses of a combined heat and power plant with absorption inlet cooling and evaporative aftercooling. Energy 2011;36:2662–70. http://dx.doi.org/10.1016/j.energy.2011.02.007.
[12] El-Sayed YM, Gaggioli RA. A critical review of second law costing methods—I: background and algebraic procedures. J Energy Resour Technol 1989;111:1–7. http://dx.doi.org/10.1115/1.3231396.
[13] Gaggioli RA, El-Sayed YM. A critical review of second law costing methods—II: calculus procedures. J Energy Resour Technol 1989;111:8–15. http://dx.doi.org/10.1115/1.3231402.
[14] Bhargava R, Negri di Montenegro G, Peretto A. Thermoeconomic analysis of an intercooled, reheat, and recuperated gas turbine for cogeneration applications—part II: part-load operation. J Eng Gas Turb Power 2002;124:892–903. http://dx.doi.org/10.1115/1.1477195.
[15] Bakhshmand SK, Saray RK, Bahlouli K, Eftekhari H, Ebrahimi A. Exergoeconomic analysis and optimization of a triple-pressure combined cycle plant using evolutionary algorithm. Energy 2015;93(Part 1):555–67. http://dx.doi.org/10.1016/j.energy.2015.09.073.
[16] Sahoo PK. Exergoeconomic analysis and optimization of a cogeneration system using evolutionary programming. Appl Therm Eng 2008;28:1580–8. http://dx.doi.org/10.1016/j.applthermaleng.2007.10.011.
[17] Oliva DG, Francesconi JA, Mussati MC, Aguirre PA. Modeling, synthesis and optimization of heat exchanger networks. Application to fuel processing systems for PEM fuel cells. Int J Hydrog Energy 2011;36:9098–114. http://dx.doi.org/10.1016/j.ijhydene.2011.04.097.
[18] Serralunga FJ, Aguirre PA, Mussati MC. Including disjunctions in real-time optimization. Ind Eng Chem Res 2014;53:17200–13. http://dx.doi.org/10.1021/ie5004619.
[19] Mores P, Rodríguez N, Scenna N, Mussati S. CO_2 capture in power plants: minimization of the investment and operating cost of the post-combustion process using MEA aqueous solution. Int J Greenh Gas Control 2012;10:148–63. http://dx.doi.org/10.1016/j.ijggc.2012.06.002.
[20] Manassaldi JI. MINLP model for the optimal design of fired heaters, Santa Fe. 2008.
[21] Manassaldi JI, Scenna NJ, Mussati SF. Optimization mathematical model for the detailed design of air cooled heat exchangers. Energy 2014;64:734–46. http://dx.doi.org/10.1016/j.energy.2013.09.062.
[22] Caballero JA, Grossmann IE. Design of distillation sequences: from conventional to fully thermally coupled distillation systems. Comput Chem Eng 2004;28:2307–29. http://dx.doi.org/10.1016/j.compchemeng.2004.04.010.
[23] Caballero JA, Grossmann IE. Structural considerations and modeling in the synthesis of heat-integrated–thermally coupled distillation sequences. Ind Eng Chem Res 2006;45:8454–74. http://dx.doi.org/10.1021/ie060030w.
[24] Onishi VC, Ravagnani MASS, Caballero JA. Simultaneous synthesis of work exchange networks with heat integration. Chem Eng Sci 2014;112:87–107. http://dx.doi.org/10.1016/j.ces.2014.03.018.
[25] Onishi VC, Ravagnani MASS, Caballero JA. MINLP model for the synthesis of heat exchanger networks with handling pressure of process streams. In: Klemeš Jiří Jaromír, Varbanov Petar Sabev, Liew Peng Yen, editors. Comput. Aided Chem. Eng., vol. 33. Elsevier; 2014. p. 163–8.
[26] Caballero JA, Navarro MA, Ruiz-Femenia R, Grossmann IE. Integration of different models in the design of chemical processes: application to the design of a power plant. Appl Energy 2014;124:256–73. http://dx.doi.org/10.1016/j.apenergy.2014.03.018.
[27] Bruno JC, Fernandez F, Castells F, Grossmann IE. A rigorous MINLP model for the optimal synthesis and operation of utility plants. Chem Eng Res Des 1998;76:246–58. http://dx.doi.org/10.1205/026387698524901.
[28] Tveit T-M, Fogelholm C-J. Multi-period steam turbine network optimisation. Part II: development of a multi-period MINLP model of a utility system. Appl Therm Eng 2006;26:1730–6. http://dx.doi.org/10.1016/j.applthermaleng.2005.11.004.
[29] Tveit T-M, Savola T, Gebremedhin A, Fogelholm C-J. Multi-period MINLP model for optimising operation and structural changes to CHP plants in district heating networks with long-term thermal storage. Energy Convers Manag 2009;50:639–47. http://dx.doi.org/10.1016/j.enconman.2008.10.010.
[30] Martelli E, Amaldi E, Consonni S. Numerical optimization of heat recovery steam cycles: mathematical model, two-stage algorithm and applications. Comput Chem Eng 2011;35:2799–823. http://dx.doi.org/10.1016/j.compchemeng.2011.04.015.
[31] Wang L, Yang Y, Dong C, Morosuk T, Tsatsaronis G. Parametric optimization of supercritical coal-fired power plants by MINLP and differential evolution. Energy Convers Manag n.d. doi:10.1016/j.enconman.2014.01.006.
[32] Kim JS, Edgar TF. Optimal scheduling of combined heat and power plants using mixed-integer nonlinear programming. Energy 2014;77:675–90. http://dx.doi.org/10.1016/j.energy.2014.09.062.
[33] Arcuri P, Beraldi P, Florio G, Fragiacomo P. Optimal design of a small size trigeneration plant in civil users: a MINLP (mixed integer non linear programming model). Energy 2015;80:628–41. http://dx.doi.org/10.1016/j.energy.2014.12.018.
[34] Mussati SF, Barttfeld M, Aguirre PA, Scenna NJ. A disjunctive programming model for superstructure optimization of power and desalting plants. Desalination 2008;222:457–65. http://dx.doi.org/10.1016/j.desal.2007.01.162.
[35] Mussati SF, Aguirre PA, Scenna NJ. A rigorous, mixed-integer, nonlineal programming model (MINLP) for synthesis and optimal operation of cogeneration seawater desalination plants. Desalination 2004;166:339–45. http://dx.doi.org/10.1016/j.desal.2004.06.088.
[36] Zhang J, Liu P, Zhou Z, Ma L, Li Z, Ni W. A mixed-integer nonlinear programming approach to the optimal design of heat network in a polygeneration energy system. Appl Energy 2014;114:146–54. http://dx.doi.org/10.1016/j.apenergy.2013.09.057.
[37] Franco A, Giannini N. A general method for the optimum design of heat recovery steam generators. Energy 2006;31:3342–61. http://dx.doi.org/10.1016/j.energy.2006.03.005.
[38] Manassaldi JI, Mussati SF, Scenna NJ. Optimal synthesis and design of heat recovery steam generation (HRSG) via mathematical programming. Energy 2011;36:475–85. http://dx.doi.org/10.1016/j.energy.2010.10.017.
[39] Carapellucci R, Giordano L. Thermoeconomic Optimization of Heat Recovery Steam Generators: A Modular Approach to Define the Layout of Heat Exchange Sections 2012:1549–59. doi:10.1115/IMECE2012-86313.
[40] Wagner W, Kretzschmar H-J. International steam tables – properties of water and steam based on the industrial formulation IAPWS-IF97: tables, algorithms, diagrams, and CD-ROM electronic steam tables – all of the equations of IAPWS-IF97 including a complete set of supplementary backward equations for fast calculations of heat cycles, boilers, and steam turbines. Springer Science & Business Media; 2007.
[41] Poling B, Prausnitz J, Connell JO. The properties of gases and liquids. McGraw Hill Professional; 2000.
[42] Casarosa C, Donatini F, Franco A. Thermoeconomic optimization of heat recovery steam generators operating parameters for combined plants. Energy 2004;29:389–414. http://dx.doi.org/10.1016/S0360-5442(02)00078-6.
[43] Ganapathy V. Steam generators and waste heat boilers: for process and plant engineers. CRC Press; 2014.
[44] Chen JJJ. Comments on improvements on a replacement for the logarithmic mean. Chem Eng Sci 1987;42:2488–9. http://dx.doi.org/10.1016/0009-2509(87)80128-8.
[45] Mussati SF, Aguirre PA, Scenna NJ. Superstructure of alternative configurations of the multistage flash desalination process. Ind Eng Chem Res 2006;45:7190–203. http://dx.doi.org/10.1021/ie051053y.
[46] Mussati SF, Aguirre PA, Scenna NJ. Novel configuration for a multistage flash-mixer desalination system. Ind Eng Chem Res 2003;42:4828–39. http://dx.doi.org/10.1021/ie020318v.
[47] Druetta P, Aguirre P, Mussati S. Optimization of multi-effect evaporation desalination plants. Desalination 2013;311:1–15. http://dx.doi.org/10.1016/j.desal.2012.10.033.
[48] Ignacio E. Grossmann, Jagadisan Viswanathan, Aldo Vecchietti, Ramesh Raman, Erwin Kalvelagen. GAMS Solvers. DICOPT n.d. http://www.gams.com/help/index.jsp?topic=%2Fgams.doc%2Fsolvers%2Findex.html.
[49] IBM ILOG. GAMS Solvers. CPLEX n.d. http://www.gams.com/help/index.jsp?topic=%2Fgams.doc%2Fsolvers%2Findex.html.
[50] Arne Drud. GAMS Solvers. CONOPT n.d. http://www.gams.com/help/index.jsp?topic=%2Fgams.doc%2Fsolvers%2Findex.html.

Nomenclature

Continuous Variables

P: Pressure [Bar]
T: Temperature [K]
m: Mass flow-rate [kg/sec]
H: Specific enthalpy [kJ/kg]
mH: Stream enthalpy [kW]
A: Heat exchanged area [m^2]
ΔT: Logarithmic means temperature difference (Chen approximation) [K]
LMTD: Logarithmic means temperature difference [K]
U: Overall heat transfer coefficient [kW/m^2K]
S: Specific entropy [kJ/kgK]
Q: Heat transfer [kW]

W: Power production or consumption [kW]
v: Specific volume [m^3/kg]
TNP: Total net power [kW]
THTA: Total heat transfer area [m^2]

Binary Variables

x: Heat exchanged existence
y: Pumps existence

Superscript

ec: Economizer
ev: Evaporator
sh: Superheater
pump: Pumps
cond: Condenser
sat: Saturated condition
st: Steam turbine
ste: Steam turbine with extraction

Subscript

i,j,k,l,m: Water stream
p,q,r: Exhaust gas stream
n,n′: Equipment number
L: Liquid state
V: Vapor state
G: Exhaust gas
lo: Lower bound
up: Upper bound